condensed matter

MDPI

Review

Functional Nanoscale Phase Separation and Intertwined Order in Quantum Complex Materials

Gaetano Campi [1,*] and Antonio Bianconi [1,2,3]

[1] Institute of Crystallography, CNR, Via Salaria Km 29,300, 00015 Monterotondo, Rome, Italy; antonio.bianconi@ricmass.eu
[2] RICMASS Rome International Center for Materials Science, Superstripes Via dei Sabelli 119A, 00185 Roma, Italy
[3] Moscow Engineering Physics Institute, National Research Nuclear University MEPhI, 115409 Moscow, Russia
* Correspondence: gaetano.campi@ic.cnr.it

Abstract: Nanoscale phase separation (NPS), characterized by particular types of correlated disorders, plays an important role in the functionality of high-temperature superconductors (HTS). Our results show that multiscale heterogeneity is an essential ingredient of quantum functionality in complex materials. Here, the interactions developing between different structural units cause dynamical spatiotemporal conformations with correlated disorder; thus, visualizing conformational landscapes is fundamental for understanding the physical properties of complex matter and requires advanced methodologies based on high-precision X-ray measurements. We discuss the connections between the dynamical correlated disorder at nanoscale and the functionality in oxygen-doped perovskite superconducting materials.

Keywords: topology; complex materials; spatial statistics

check for updates

Citation: Campi, G.; Bianconi, A. Functional Nanoscale Phase Separation and Intertwined Order in Quantum Complex Materials. *Condens. Matter* **2021**, *6*, 40. https://doi.org/10.3390/condmat6040040

Academic Editor: Alessandro Scordo

Received: 14 October 2021
Accepted: 2 November 2021
Published: 5 November 2021

Publisher's Note: MDPI stays neutral with regard to jurisdictional claims in published maps and institutional affiliations.

Copyright: © 2021 by the authors. Licensee MDPI, Basel, Switzerland. This article is an open access article distributed under the terms and conditions of the Creative Commons Attribution (CC BY) license (https://creativecommons.org/licenses/by/4.0/).

1. Introduction

Nanoscale phase separation (NPS) has been considered to be detrimental for high-temperature superconductivity. However, high-precision X-ray measurements in solid-state physics [1–5] have recently provided experimental validation for the alternative paradigm, where lattice heterogeneity from the atomic limit to the micron scale plays a key role [6–12]. NPS shows that intertwined and interlocked nanoscale lattice structures form heterostructures at the atomic limit [13]. This induces the emergence of novel functionalities, such as high-temperature superconductivity, in complex quantum materials as organics [13–20], doped perovskites [21–39], iron-based superconductors [40–44], charge–density–wave materials [45–52], manganites showing colossal magnetoresistance [53–57], doped diborides [58–60], smart structures and biological systems [61–66], perovskite oxide interfaces [67–69], and magnetic materials [70,71].

Today, at the beginning of the twenties of the XXI century, the development of advanced experimental X-ray methods has provided evidence that quantum functionalities (e.g., colossal magnetoresistance and high-temperature superconductivity) are controlled by the correlated lattice disorder from atomic scales to micron scales. This multiscale lattice heterogeneity has been quite difficult to unveil by conventional experimental approaches, requiring high spatial resolution probes. Nowadays, advanced, latest generation synchrotron sources and new X-ray optics have allowed the design of new scanning techniques, based on focused X-ray beams.

In this way, several crystallographic structures, coexisting on micron scales and nanoscales, have been visualized in high-temperature superconductors (HTS). Strain and doping drive these systems at critical points for phase separation, with the coexistence of different crystallographic phases existing in different nanoregions of the crystal. While in the literature on HTS, the focus of theoretical research has been addressed to electronic

phase separation and inhomogeneity—due to competition or intertwining between superconductivity and magnetism—the main result of scanning X-ray diffraction has been to provide compelling experimental evidence that, at nanoscale, different puddles show a substantial lattice structural difference, which necessarily implies electronic and magnetic phase separation. In fact, looking at the nanoscale, we have observed different nanoregions with different lattice structures, showing different electronic and magnetic ordered phases, with different topologies that influence the Fermi surfaces, the pseudogap energy, and even the superconducting critical temperature. We would like to underline archetypal cases of intrinsic phase separation in $A_xFe_{2-y}Se_2$, which are originated by the coexistence of an insulating magnetic phase and a paramagnetic metallic phase with an in-plane compressed and expanded lattice [40–44]. A second clear case of phase separation has been found in $YBa_2Cu_3O_{6+y}$, with $y < 0.5$, where superconductivity ($y > 0.33$) percolates in a network of oxygen-ordered nanoregions ($y = 0.5$), interspersed with oxygen-depleted domains ($y = 0$) [37].

Here, we have chosen to discuss the relationship between phase separation at nanoscale and the emerging macroscopic properties in two high-temperature superconducting quantum materials, such as $La_2CuO_{4.1}$ [38] and $HgBa_2CuO_{4.12}$ [7], doped by mobile oxygen interstitial ions (O-i).

2. Results

2.1. Correlated Disorder and Phase Separation in La_2CuO_{4+y}

La_2CuO_{4+y} is one of the simplest compounds, where y oxygen interstitial ions (O-i) in the rocksalt [La_2O_{2+y}] are intercalated by [CuO_2] layers. Thanks to the high synchrotron photon flux, we have measured the satellite peaks, which are associated with super-cells, due to oxygen interstitial O-i dopants and charge–density waves (CDW) arrangement (see Figure 1a). CDWs incommensurate diffuse satellites with wave vector $\mathbf{q_{CDW}} = 0.21\mathbf{b^*} + 0.29\mathbf{c^*}$, coexist with O-i satellites displaced by $\mathbf{q_{O\text{-}i}} = 0.25\mathbf{b^*} + 0.5\mathbf{c^*}$. Oxygen ions, O-i. and CDW superstructures are characterized by a different staging, that is, their c* component; indeed, O-i and CDW have staging $\mathbf{c^*} = 0.5$ and $\mathbf{c^*} = 0.29$, respectively, as indicated by the white arrows in Figure 1a.

A common and intriguing feature of quantum materials is that their emerging properties can be easily manipulated by weak external stimuli, such as temperature gradient, strain, and photon illumination. Due to the mobility of oxygen interstitials (O-i), our systems present structural conformational landscapes. The conformations have been manipulated by continuous X-ray photo illumination, as shown in Figure 1b, where we bring the sample from a structural conformation with disordered O-i to a different conformation with ordered O-i, after illumination. Different conformations, characterized by different order degrees of O-i [72,73], can be obtained by combining X-ray flux intensity with thermal cycling, as shown in Figure 1c. Here the (full symbols) X-ray low flux and (empty symbols) high flux on the sample, correspond to 0.5×10^{14} photons s^{-1} cm^{-2} and 5.0×10^{14} photons s^{-1} cm^{-2}, respectively. The temperature change rate has been 1 K min^{-1} in both low-flux and high-flux illumination. Each point on the two hysteresis corresponds with a specific structural conformation, with a specific degree of order (or disorder) of O-i.

The different O-i ordered domains are inhomogeneously distributed in space, as seen by SμXRD. The maps in Figure 2a,b show two different O-i distributions, obtained with two different thermal treatments; the first one (a) shows the maximum critical temperature ($T_c = 40$ K) and the second (b) presents a macroscopic phase separation with two critical temperatures, $T_c = 16$ K and 32 K [6].

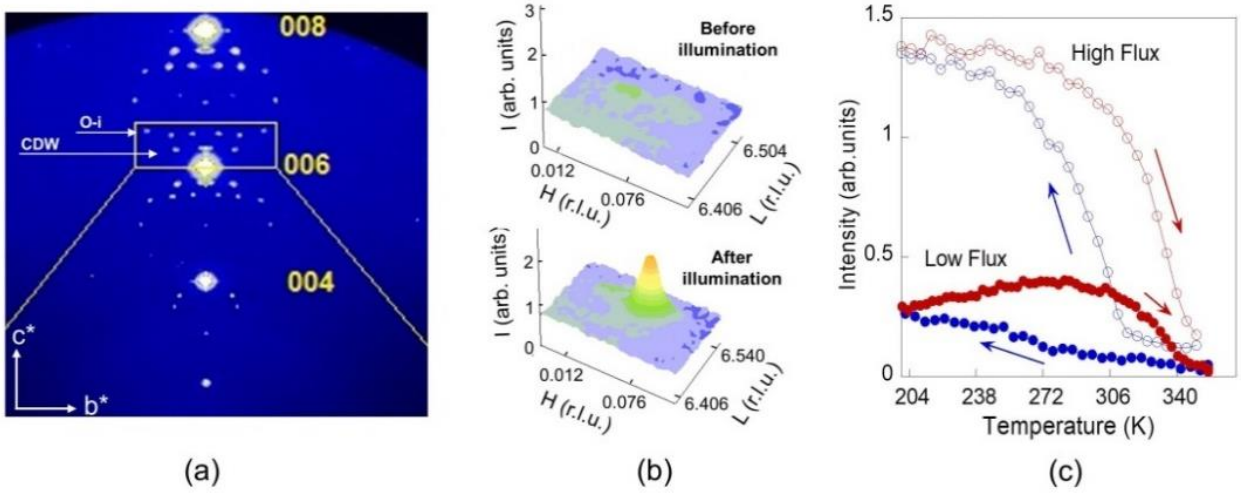

Figure 1. (**a**) XRD image of b*c* plane in the reciprocal lattice of the $La_2CuO_{4.1}$ sample. We observed several superstructures surrounding the indicated Bragg peaks (004, 006, 008), due to O-i ordering and charge–density waves (CDW). The arrows indicate the O-i and CDW superlattices. (**b**) At T = 330 K, the O-i get disordered in the sample and the diffraction satellite vanishes (upper panel). X-ray photon illumination (O-i) allows a speeding up in the ordering kinetic (lower panel). (**c**) The oxygen ordering rate depends on the X-ray flux, as shown in the thermal cycle measured by using two different X-ray photon fluxes [72]. Red and blue symbols refer to heating and cooling cycles, respectively.

We have characterized this inhomogeneity by using spatial statistics tools, described in [6]. In both samples, the probability density function of O-i satellite intensity follows an exponentially truncated power–law distribution, given by $P(x) = x^{-\alpha}\exp(-x/x_0)$, where α is the critical exponent and x_0 is the cut-off. The critical exponent, α, results to be 2.6, both in the high-T_c (a) and low-T_c (b) conformations, indicating the fractal nature of O-i arrangement. On the other hand, the cut-off, x_0, is larger for the high-T_c = 40 K sample, as can be seen in Figure 2c. This means that a larger extent of O-i satellite intensity with fractal geometry favors a higher T_c [38].

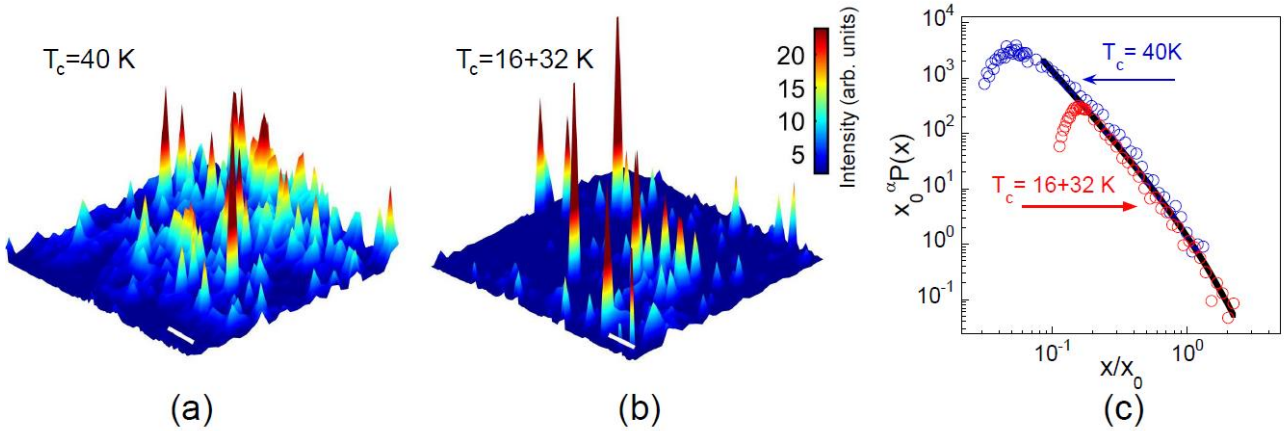

Figure 2. Spatial distribution of the O-i superstructure intensity for two different conformations in $La_2Cu0_{4.1}$ samples, with (**a**) T_c = 40 K (**b**) and T_c = 16 and 32 K phases in a 500 × 400 μm^2 area. The bar corresponds to 50 μm. (**c**) The rescaled probability distribution, $x^{\alpha}P(x)$, of the O-i superstructure intensity for the two samples. The cut-off, x_0, increases from 8 ± 1 in the low-T_c conformation to 31 ± 2 in the high-T_c conformation. The rescaled distributions collapse on the same universal curve (black solid line) [38].

We have found that the spatial inhomogeneity is characterized by a strong spatial anticorrelation between the O-i-rich and CDW-rich regions. In the oxygen-rich regions, the system is in the over-doped metallic phase, while in the oxygen-poor region in the underdoped phase, we measure a high density of CDW. Figure 3a shows the map of

difference between the intensity of O-i and CDW diffraction satellites. The O-i are located in the 1/4,1/4,1/4 site, and form commensurate stripes in the La_2O_2 structure, intertwined with incommensurate lattice CDW domains [39]. Indeed, we observed micron size puddles of blue metallic oxygen-rich regions, separated by red CDW-rich zones, by a filamentary percolating interface, indicated by white space in Figure 3b.

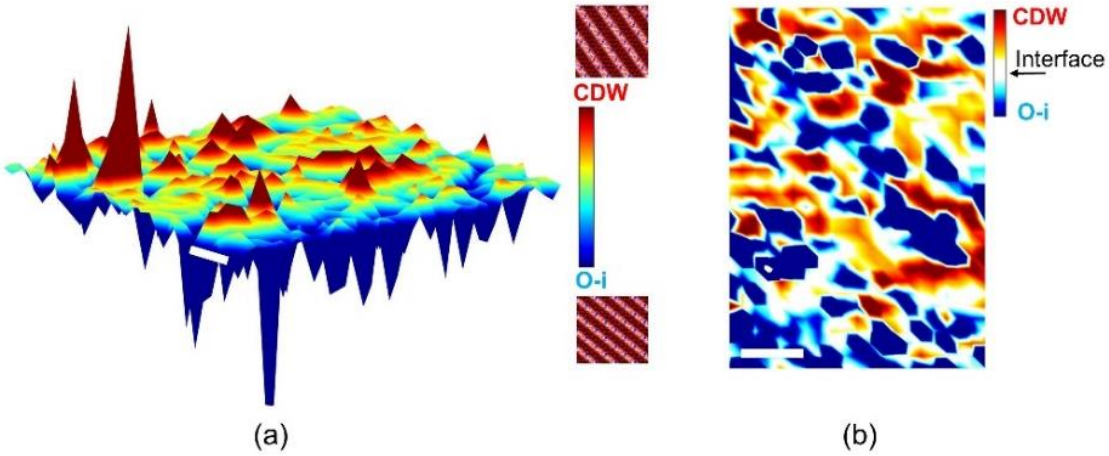

Figure 3. (**a**) Surface plot of the map difference between the normalized intensities of both CDW and O-i satellites in $La_2Cu0_{4.1}$ [38]. CDW puddles are dominant in red regions, while the O-i stripes are dominant in the blue zones. The lattice modulations corresponding to CDWs and O-i superstructures are depicted. (**b**) 2D map difference highlighting the interface (white region) between CDW-rich and O-i-rich regions. The white bars correspond to 5 μm.

2.2. Correlated Disorder and Phase Separation in $HgBa_2CuO_{4+y}$

Structural and electronic inhomogeneity has been studied in the high-temperature perovskite superconductor, with tetragonal crystal symmetry $HgBa_2CuO_{4+y}$ with a single CuO_2 plane. In this compound, the oxygen interstitial ions (O-i) form atomic stripes in the spacer layer [$HgO_yBa_2O_2$] between [CuO_2] planes. We have measured the diffuse scattering associated with both CDW and oxygen interstitial arrangement in the lattice. Diffuse CDW satellites have been detected at $\mathbf{q_{CDW}} = 0.23\mathbf{a^*} + 0.16\mathbf{c^*}$ and $\mathbf{q_{CDW}} = 0.23\mathbf{b^*} + 0.16\mathbf{c^*}$ (where $\mathbf{a^*}$, $\mathbf{b^*}$, and $\mathbf{c^*}$ are the lattice units in the reciprocal space) around the (108) Bragg peak, below the onset temperature $T_{CDW} = 240$ K [7]. Resolution-limited streaks connecting the Bragg peaks, due to atomic O-i stripes in the HgO_y spacer layers, have been measured in agreement with previous experiments [6,32].

In Figure 4a,b we show the maps of the integrated intensity of CDW peak and oxygen O-i diffuse streaks, respectively [7,9], as seen by SμXRD measurements. Both O-i and CDW maps are spatially inhomogeneous, and their PDF is well modeled by a power–law behavior also in this case, as shown in Figure 4c. The critical exponents in the two intensity distributions are 1.8 ± 0.1 and 2.2 ± 0.1 for the O-i and CDW, respectively [7].

A map of the spatial organization of the in-plane CDW-puddle size, ξ_a, is shown in Figure 4d. Although the average size of CDW puddles is 4.3 nm (in agreement with previous works), its probability density function, shown in Figure 4e, has a fat-tail, fitted by a power–law curve with critical exponent of 2.8 ± 0.1. This means that rare and larger puddles up to 40 nm are measured, and their distribution provides a complex topology for the flowing of superconductivity currents [7,9].

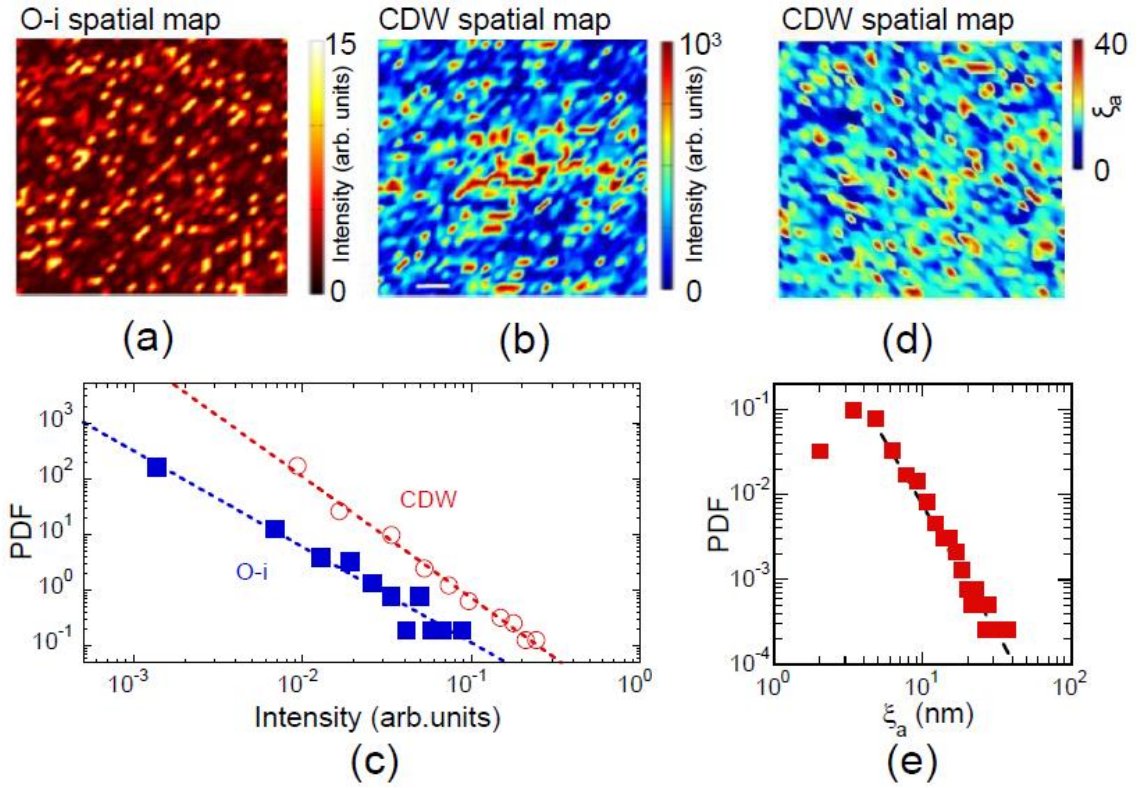

Figure 4. Colour plot of the map of the (**a**) O-i streak intensity and (**b**) charge–density waves (CDW) peak in $HgBa_2CuO_{4.12}$. (**c**) Probability density function, calculated from the O-i streaks and CDW intensity map in (**a**,**b**), showing a power–law behaviour. (**d**) Colour map of the CDW coherence length ξ_a of the CDW. (**e**) Probability density distribution of ξ_a.

As in the La_2CuO_{4+y} superconductor, the spatial inhomogeneity shows a negative correlation between O-i and CDW. This is well depicted in the 'difference map' between CDW peaks and O-i-diffuse streaks in Figure 5a. The poor CDW regions on the CuO_2 basal plane correspond to O-i-rich regions on the HgO_y layers. The O-i atomic striped domains are here intertwined with incommensurate lattice CDW. The percolating filamentary interface between O-i-rich and O-i-poor regions is indicated by white space in Figure 5b.

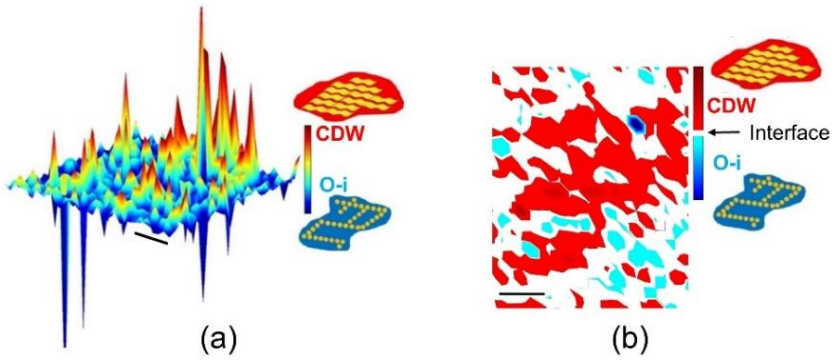

Figure 5. (**a**) Surface plot of the map difference between the normalized intensities of both CDW satellite and O-i streaks in $HgBa_2CuO_{4.12}$ [7]. CDW puddles are dominant in red regions and the O-i stripes are dominant in the blue zones. The bar corresponds to 5 μm. (**b**) Pictorial view of the spatial anticorrelation between CDW puddles in the CuO_2 plane and the O-i-rich domains in the HgO_y layers. Here, the interface space between CDW and O-i has been highlighted by the white region. The bar corresponds to 5 μm.

3. Discussion

The anomalous phase diagram of HTS cuprates is believed, nowadays, to be closely related to the phase separation at multiple scale length. This feature is particularly pronounced in those compounds doped by mobile oxygen interstitials. In this context, the present work reports evidence of nanoscale phase separation in the cases of two different oxygen-doped layered perovskites, La_2CuO_{4+y} and $HgBa_2CuO_{4+y.}$ At optimum doping level, specific charge ordering and segregation lead to the formation of metallic and insulating domains with oxygen-rich and oxygen-poor regions, respectively. These different zones have been measured as different superlattices in X-ray diffraction and their inhomogeneous spatial distribution has been visualized by scanning micro X-ray diffraction. The results provide relevant evidence for the universality of phase separation, where dopants' O-i-rich domains are intertwined with CDW domains, even in the most optimized superconducting cuprates.

We have shown that the coexisting phases can be easily manipulated (e.g., by X-ray illumination) on controlled small areas, drawing a way to extend the functionality of the investigated materials in the direction of information storage [74,75].

4. Materials and Methods

The La_2CuO_{4+y} (LCO) single crystal with y = 0.1 has orthorhombic *Fmmm* space group symmetry, with lattice parameters a = (5.386 $\pm$ 0.004) Å, b = (5.345 $\pm$ 0.008) Å, and c = (13.205 $\pm$ 0.031) Å at room temperature. The $HgBa_2CuO_{4+y}$ (Hg1201) single crystal, with y = 0.12, has a sharp superconducting transition at T_c = 95 K. The crystal structure has tetragonal P4/mmm space group symmetry with lattice parameters a = b = 0.387480(5) nm and c = 0.95078(2) nm at T = 100 K. Diffraction measurements on both single crystals of LCO and Hg1201 were performed on the ID13 beamline at ESRF, as described in [38] and [7], respectively. Data analysis has been performed by using customized and homemade written MATLAB routines [6].

Author Contributions: G.C. and A.B. conceived the experiments and wrote the paper. All authors have read and agreed to the published version of the manuscript.

Funding: This research received no external funding.

Institutional Review Board Statement: Not applicable.

Informed Consent Statement: Not applicable.

Data Availability Statement: Data can be requested to the authors.

Acknowledgments: The authors thank Luisa Barba and XRD1 beamline staff at ELETTRA, Trieste, Italy; Manfred Burghammer and ID13 beamline staff at ESRF; Alessandro Ricci, Nicola Poccia, Michela Fratini, and Stefano Agrestini for the long-standing collaboration.

Conflicts of Interest: The authors declare no conflict of interest.

References

1. Schunck, J.O.; Döring, F.; Rösner, B.; Buck, J.; Engel, R.Y.; Miedema, P.S.; Mahatha, S.K.; Hoesch, M.; Petraru, A.; Kohlstedt, H.; et al. Soft X-ray imaging spectroscopy with micrometer resolution. *Optica* **2021**, *8*, 156–160. [CrossRef]
2. Schülli, T.U.; Leake, S.J. X-ray nanobeam diffraction imaging of materials. *Curr. Opin. Solid State Mater. Sci.* **2018**, *22*, 188–201. [CrossRef]
3. Campi, G. Structural Fluctuations at Nanoscale in Complex Functional Materials. In *Synchrotron Radiation Science and Applications*; Springer: Cham, Switzerland, 2021; pp. 181–189.
4. Poccia, N.; Chorro, M.; Ricci, A.; Xu, W.; Marcelli, A.; Campi, G.; Bianconi, A. Percolative superconductivity in $La_2CuO_{4.06}$ by lattice granularity patterns with scanning micro X-ray absorption near edge structure. *Appl. Phys. Lett.* **2014**, *104*, 221903. [CrossRef]
5. Campi, G.; Ricci, A.; Poccia, N.; Fratini, M.; Bianconi, A. X-rays Writing/Reading of charge density waves in the CuO_2 plane of a simple cuprate superconductor. *Condens. Matter.* **2017**, *2*, 26. [CrossRef]
6. Campi, G.; Bianconi, A. Evolution of complexity in out-of-equilibrium systems by time-resolved or space-resolved synchrotron radiation techniques. *Condens. Matter.* **2019**, *4*, 32. [CrossRef]

7. Campi, G.; Bianconi, A.; Poccia, N.; Bianconi, G.; Barba, L.; Arrighetti, G.; Innocenti, D.; Karpinski, J.; Zhigadlo, N.D.; Kazakov, S.M.; et al. Inhomogeneity of charge-density-wave order and quenched disorder in a high-Tc superconductor. *Nature* **2015**, *525*, 359–362. [CrossRef]
8. Dagotto, E. Complexity in strongly correlated electronic systems. *Science* **2005**, *309*, 257–262. [CrossRef]
9. Campi, G.; Bianconi, A. High-Temperature Superconductivity in a Hyperbolic Geometry of Complex Matter from Nanoscale to Mesoscopic Scale. *J. Supercond. Nov. Magn.* **2016**, *29*, 627–631. [CrossRef]
10. Carlson, E.W. Condensed-matter physics: Charge topology in superconductors. *Nature* **2015**, *525*, 329–330. [CrossRef]
11. Bishop, A.R. HTC oxides: A collusion of spin, charge and lattice. *J. Phys. Conf. Ser.* **2008**, *108*, 012027. [CrossRef]
12. Littlewood, P. Superconductivity: An X-ray oxygen regulator. *Nat. Mater.* **2011**, *10*, 726–727. [CrossRef]
13. Amabilino, D.B.; Stoddart, J.F. Interlocked and intertwined structures and superstructures. *Chem. Rev.* **1995**, *95*, 2725–2828. [CrossRef]
14. Živković, J.M.; Stanković, I.M.; Ninković, D.B.; Zarić, S.D. Decisive Influence of Environment on Aromatic/Aromatic Interaction Geometries. Comparison of Aromatic/Aromatic Interactions in Crystal Structures of Small Molecules and in Protein Structures. *Cryst. Growth Des.* **2021**, *21*, 1898–1904. [CrossRef]
15. Mazziotti, M.V.; Valletta, A.; Campi, G.; Innocenti, D.; Perali, A.; Bianconi, A. Possible Fano resonance for high-Tc multi-gap superconductivity in p-Terphenyl doped by K at the Lifshitz transition. *EPL Europhys. Lett.* **2017**, *118*, 3700. [CrossRef]
16. Mazziotti, M.V.; Jarlborg, T.; Bianconi, A.; Valletta, A. Room temperature superconductivity dome at a Fano resonance in superlattices of wires. *EPL Europhys. Lett.* **2021**, *134*, 17001. [CrossRef]
17. Mazziotti, M.V.; Raimondi, R.; Valletta, A.; Campi, G.; Bianconi, A. Resonant multigap superconductivity at room temperature near a Lifshitz topological transition in sulfur hydrides. *arXiv* **2021**, arXiv:2106.14394.
18. Bianconi, A.; Jarlborg, T. Lifshitz transitions and zero point lattice fluctuations in sulfur hydride showing near room temperature superconductivity. *Nov. Supercond. Mater.* **2015**, *1*, 37–49. [CrossRef]
19. Cui, Y.; Li, B.; He, H.; Zhou, W.; Chen, B.; Qian, G. Metalorganic frameworks as platforms for functional materials. *Acc. Chem. Res.* **2016**, *49*, 483–493. [CrossRef]
20. Kochev, V.D.; Kesharpu, K.K.; Grigoriev, P.D. Anisotropic zero-resistance onset in organic superconductors. *Phys. Rev. B* **2021**, *103*, 014519. [CrossRef]
21. Bianconi, A.; Missori, M. High Tc superconductivity by quantum confinement. *J. Phys. I* **1994**, *4*, 361–365.
22. Bianconi, A. On the possibility of new high Tc superconductors by producing metal heterostructures as in the cuprate perovskites. *Solid State Commun.* **1994**, *89*, 933–936. [CrossRef]
23. Bianconi, A.; Missori, M.; Oyanagi, H.; Yamaguchi, H.; Ha, D.H.; Nishiara, Y.; Della Longa, S. The measurement of the polaron size in the metallic phase of cuprate superconductors. *EPL Europhys. Lett.* **1995**, *31*, 41. [CrossRef]
24. Della Longa, S.; Soldatov, A.; Pompa, M.; Bianconi, A. Atomic and electronic structure probed by X-ray absorption spectroscopy: Full multiple scattering analysis with the G4XANES package. *Comput. Mater. Sci.* **1995**, *4*, 199–210. [CrossRef]
25. Saini, N.L.; Lanzara, A.; Missori, M.; Rossetti, T.; Bianconi, A.; Oyanagi, H.; Yamaguchi, H.; Oka, K.; Ito, T. Local lattice instability of CuO_2 plane in La1.85 Sr0.15 CuO_4 by polarized Cu K edge absorption. *Phys. C Supercond.* **1995**, *251*, 383–388. [CrossRef]
26. Bianconi, A.; Saini, N.L.; Rossetti, T.; Lanzara, A.; Perali, A.; Missori, M.; Oyanagi, H.; Yamaguchi, H.; Nishihara, Y.; Ha, D.H. Stripe structure in the CuO_2 plane of perovskite superconductors. *Phys. Rev. B* **1996**, *54*, 12018. [CrossRef]
27. Bianconi, A.; Saini, N.L.; Lanzara, A.; Missori, M.; Rossetti, T.; Oyanagi, H.; Yamaguchi, H.; Oka, K.; Ito, T. Determination of the Local Lattice Distortions in the CuO_2 Plane of La1.85Sr0.15CuO4. *Phys. Rev. Lett.* **1996**, *76*, 3412. [CrossRef]
28. Saini, N.L.; Oyanagi, H.; Ito, T.; Scagnoli, V.; Filippi, M.; Agrestini, S.; Campi, G.; Oka, K.; Bianconi, A. Temperature dependent local Cu-O displacements from underdoped to overdoped La-Sr-Cu-O superconductor. *Eur. Phys. J. B Condens. Matter. Complex Syst.* **2003**, *36*, 75–80. [CrossRef]
29. Bianconi, A. Shape resonances in superstripes. *Nat. Phys.* **2013**, *9*, 536–537. [CrossRef]
30. Krockenberger, Y.; Ikeda, A.; Yamamoto, H. Atomic Stripe Formation in Infinite-Layer Cuprates. *ACS Omega* **2021**, *6*, 21884–21891. [CrossRef]
31. Hsu, C.C.; Huang, B.C.; Schnedler, M.; Lai, M.Y.; Wang, Y.L.; Dunin-Borkowski, R.E.; Chang, C.S.; Lee, T.K.; Ebert, P.; Chiu, Y.P. Atomically-resolved interlayer charge ordering and its interplay with superconductivity in $YBa_2Cu_3O_{6.81}$. *Nat. Commun.* **2021**, *12*, 1–8. [CrossRef]
32. Izquierdo, M.; Freitas, D.C.; Colson, D.; Garbarino, G.; Forget, A.; Raffy, H.; Itié, J.P.; Ravy, S.; Fertey, P.; Núñez-Regueiro, M. Charge Order and Suppression of Superconductivity in $HgBa_2CuO_{4+d}$ at High Pressures. *Condens. Matter.* **2021**, *6*, 25. [CrossRef]
33. Ohgoe, T.; Hirayama, M.; Misawa, T.; Ido, K.; Yamaji, Y.; Imada, M. Ab initio study of superconductivity and inhomogeneity in a Hg-based cuprate superconductor. *Phys. Rev. B* **2020**, *101*, 045124. [CrossRef]
34. Bianconi, A. Shape resonances in multi-condensate granular superconductors formed by networks of nanoscale-striped puddles. *J. Phys. Conf. Ser.* **2013**, *449*, 012002. [CrossRef]
35. Jarlborg, T.; Bianconi, A. Fermi surface reconstruction of superoxygenated La_2CuO_4 superconductors with ordered oxygen interstitials. *Phys. Rev. B* **2013**, *87*, 054514. [CrossRef]
36. Ricci, A.; Poccia, N.; Campi, G.; Coneri, F.; Barba, L.; Arrighetti, G.; Polentarutti, M.; Burghammer, M.; Sprung, M.; v Zimmermann, M.; et al. Networks of superconducting nano-puddles in 1/8 doped $YBa_2Cu_3O_{6.5+y}$ controlled by thermal manipulation. *N. J. Phys.* **2014**, *16*, 053030. [CrossRef]

37. Campi, G.; Ricci, A.; Poccia, N.; Barba, L.; Arrighetti, G.; Burghammer, M.; Caporale, A.S.; Bianconi, A. Scanning micro-X-ray diffraction unveils the distribution of oxygen chain nanoscale puddles in $YBa_2Cu_3O_{6.33}$. *Phys. Rev. B* **2013**, *87*, 014517. [CrossRef]
38. Fratini, M.; Poccia, N.; Ricci, A.; Campi, G.; Burghammer, M.; Aeppli, G.; Bianconi, A. Scale-free structural organization of oxygen interstitials in La_2CuO_{4+y}. *Nature* **2010**, *466*, 841–844. [CrossRef] [PubMed]
39. Poccia, N.; Ricci, A.; Campi, G.; Fratini, M.; Puri, A.; Di Gioacchino, D.; Marcelli, A.; Reynolds, M.; Burghammer, M.; Saini, N.L.; et al. Optimum inhomogeneity of local lattice distortions in La_2CuO_{4+y}. *Proc. Natl. Acad. Sci. USA* **2012**, *109*, 15685–15690. [CrossRef]
40. Ricci, A.; Poccia, N.; Joseph, B.; Innocenti, D.; Campi, G.; Zozulya, A.; Westermeier, F.; Schavkan, A.; Coneri, F.; Bianconi, A.; et al. Direct observation of nanoscale interface phase in the superconducting chalcogenide $KxFe_2$-ySe_2 with intrinsic phase separation. *Phys. Rev. B* **2015**, *91*, 020503. [CrossRef]
41. Ricci, A.; Joseph, B.; Poccia, N.; Campi, G.; Saini, N.L.; Bianconi, A. Temperature Dependence of $\sqrt{2}$ x $\sqrt{2}$ Phase in Superconducting $K_{0.8}Fe_{1.6}Se_2$ Single Crystal. *J. Supercond. Nov. Magn.* **2014**, *27*, 1003–1007. [CrossRef]
42. Weyeneth, S.; Bendele, M.; Von Rohr, F.; Dluzewski, P.; Puzniak, R.; Krzton-Maziopa, A.; Bosma, S.; Guguchia, Z.; Khasanov, R.; Shermadini, Z.; et al. Superconductivity and magnetism in $Rb_xFe_{2-y}Se_2$: Impact of thermal treatment on mesoscopic phase separation. *Phys. Rev. B* **2012**, *86*, 134530. [CrossRef]
43. Krzton-Maziopa, A.; Svitlyk, V.; Pomjakushina, E.; Puzniak, R.; Conder, K. Superconductivity in alkali metal intercalated iron selenides. *J. Phys. Condens. Matter.* **2016**, *28*, 293002. [CrossRef] [PubMed]
44. Hazi, J.; Mousavi, T.; Dudin, P.; van der Laan, G.; Maccherozzi, F.; Krzton-Maziopa, A.; Pomjakushina, E.; Conder, K.; Speller, S.C. Magnetic imaging of antiferromagnetic and superconducting phases in $Rb_xFe_{2-y}Se_2$ crystals. *Phys. Rev. B* **2018**, *97*, 054509. [CrossRef]
45. Gebreyohannes, M.G.; Singh, P. Possible coexistence of charge density wave and superconductivity and enhancement of the transition temperature for the layered quasi-two-dimensional superconductor 2H-$NbSe_2$. *J. Phys. Commun.* **2021**, *5*, 105010. [CrossRef]
46. Kinyanjui, M.K.; Ebad-Allah, J.; Krottenmüller, M.; Kuntscher, C.A. Atomic-scale mapping of pressure-induced deformations and phase defects in the charge density wave order parameter. *Phys. Rev. B* **2021**, *104*, 125106. [CrossRef]
47. Lee, J.; Nagao, M.; Mizuguchi, Y.; Ruff, J. Direct observation of an incommensurate charge density wave in the BiS_2-based superconductor $NdO_{1-x}FxBiS_2$. *Phys. Rev. B* **2021**, *103*, 245120. [CrossRef]
48. Grandadam, M.; Pépin, C. Pole structure of the electronic self-energy with coexistence of charge order and superconductivity. *Phys. Rev. B* **2021**, *103*, 224507. [CrossRef]
49. Huang, H.Y.; Singh, A.; Mou, C.Y.; Johnston, S.; Kemper, A.F.; Brink, J.; Chen, P.J.; Lee, T.K.; Okamoto, J.; Chu, Y.Y.; et al. Quantum fluctuations of charge order induce phonon softening in a superconducting cuprate. *arXiv* **2021**, arXiv:2108.11425.
50. Zhao, H.; Porter, Z.; Chen, X.; Wilson, S.D.; Wang, Z.; Zeljkovic, I. Imaging antiferromagnetic domain fluctuations and the effect of atomic-scale disorder in a doped spin-orbit Mott insulator. *arXiv* **2021**, arXiv:2105.12648.
51. Mukhin, S.I. Euclidean Q-balls of fluctuating SDW/CDW in the 'nested' Hubbard model of high-Tc superconductors as the origin of pseudogap and superconducting behavior. *arXiv* **2021**, arXiv:2108.10372.
52. Banerjee, S.; Atkinson, W.A.; Kampf, A.P. Emergent charge order from correlated electron-phonon physics in cuprates. *Commun. Phys.* **2020**, *3*, 1–8. [CrossRef]
53. Uehara, M.; Mori, S.; Chen, C.H.; Cheong, S.W. Percolative phase separation underlies colossal magnetoresistance in mixed-valent manganites. *Nature* **1999**, *399*, 560–563. [CrossRef]
54. Tokura, Y. Critical features of colossal magnetoresistive manganites. *Rep. Prog. Phys.* **2006**, *69*, 797–851. [CrossRef]
55. Dagotto, E. *Nanoscale Phase Separation and Colossal Magnetoresistance: The Physics of Manganites and Related Compounds*; Springer Science & Business Media: Berlin/Heidelberg, Germany, 2003.
56. Saxena, A.; Aeppli, G. Phase transitions at the nanoscale in functional materials. *MRS Bull.* **2009**, *34*, 804–813. [CrossRef]
57. Bryant, B.; Renner, C.; Tokunaga, Y.; Tokura, Y.; Aeppli, G. Imaging oxygen defects and their motion at a manganite surface. *Nat. Commun.* **2011**, *2*, 212. [CrossRef]
58. Campi, G.; Cappelluti, E.; Proffen, T.; Qiu, X.; Bozin, E.S.; Billinge, S.J.L.; Agrestini, S.; Saini, N.L.; Bianconi, A. Study of temperature dependent atomic correlations in MgB_2. *Eur. Phys. J. B* **2006**, *52*, 15–21. [CrossRef]
59. Agrestini, S.; Metallo, C.; Filippi, M.; Simonelli, L.; Campi, G.; Sanipoli, C.; Liarokapis, E.; De Negri, S.; Giovannini, M.; Saccone, A.; et al. Substitution of Sc for Mg in MgB_2: Effects on transition temperature and Kohn anomaly. *Phys. Rev. B* **2004**, *70*, 134514. [CrossRef]
60. Bauer, E.; Paul, C.; Berger, S.; Majumdar, S.; Michor, H.; Giovannini, M.; Saccone, A.; Bianconi, A. Thermal conductivity of superconducting MgB_2. *J. Phys. Condens. Matter.* **2001**, *13*, L487. [CrossRef]
61. Wadhawan, V.K. *Smart Structures: Blurring the Distinction Between the Living and the Nonliving*; Monographs on the Physics and Chemistry of Materials 65; Oxford University Press: Oxford, UK, 2007.
62. Campi, G.; Fratini, M.; Bukreeva, I.; Ciasca, G.; Burghammer, M.; Brun, F.; Tromba, G.; Mastrogiacomo, M.; Cedola, A. Imaging collagen packing dynamics during mineralization of engineered bone tissue. *Acta Biomater.* **2015**, *23*, 309–316. [CrossRef]
63. Bukreeva, I.; Campi, G.; Fratini, M.; Spanò, R.; Bucci, D.; Battaglia, G.; Giove, F.; Bravin, A.; Uccelli, A.; Venturi, C.; et al. Quantitative 3D investigation of Neuronal network in mouse spinal cord model. *Sci. Rep.* **2017**, *7*, 1–10. [CrossRef]

64. Ciasca, G.; Campi, G.; Battisti, A.; Rea, G.; Rodio, M.; Papi, M.; Pernot, P.; Tenenbaum, A.; Bianconi, A. Continuous thermal collapse of the intrinsically disordered protein tau is driven by its entropic flexible domain. *Langmuir* **2012**, *28*, 13405–13410. [CrossRef]
65. Ciasca, G.; Papi, M.; Chiarpotto, M.; Rodio, M.; Campi, G.; Rossi, C.; De Sole, P.; Bianconi, A. Transient state kinetic investigation of ferritin iron release. *Appl. Phys. Lett.* **2012**, *100*, 073703. [CrossRef]
66. Campi, G.; Cristofaro, F.; Pani, G.; Fratini, M.; Pascucci, B.; Corsetto, P.A.; Weinhausen, B.; Cedola, A.; Rizzo, A.M.; Visai, L.; et al. Heterogeneous and self-organizing mineralization of bone matrix promoted by hydroxyapatite nanoparticles. *Nanoscale* **2017**, *9*, 17274–17283. [CrossRef]
67. Mannhart, J.; Schlom, D.G. Oxide interfaces an opportunity for electronics. *Science* **2010**, *327*, 1607–1611. [CrossRef]
68. Hwang, H.Y.; Iwasa, Y.; Kawasaki, M.; Keimer, B.; Nagaosa, N.; Tokura, Y. Emergent phenomena at oxide interfaces. *Nat. Mater.* **2012**, *11*, 103–113. [CrossRef]
69. Bert, J.A.; Kalisky, B.; Bell, C.; Kim, M.; Hikita, Y.; Hwang, H.Y.; Moler, K.A. Direct imaging of the coexistence of ferromagnetism and superconductivity at the $LaAlO_3/SrTiO_3$ interface. *Nat. Phys.* **2011**, *7*, 767–771. [CrossRef]
70. Drees, Y.; Li, Z.W.; Ricci, A.; Rotter, M.; Schmidt, W.; Lamago, D.; Sobolev, O.; Rutt, U.; Gutowski, O.; Sprung, M.; et al. Hour-glass magnetic excitations induced by nanoscopic phase separation in cobalt oxides. *Nat. Commun.* **2014**, *5*, 5731. [CrossRef]
71. Campi, G.; Poccia, N.; Joseph, B.; Bianconi, A.; Mishra, S.; Lee, J.; Roy, S.; Nugroho, A.A.; Buchholz, M.; Braden, M.; et al. Direct visualization of spatial inhomogeneity of spin stripes order in $La_{1.72}Sr_{0.28}NiO_4$. *Condens. Matter.* **2019**, *4*, 77. [CrossRef]
72. Poccia, N.; Bianconi, A.; Campi, G.; Fratini, M.; Ricci, A. Size evolution of the oxygen interstitial nanowires in La_2CuO_{4+y} by thermal treatments and X-ray continuous illumination. *Supercond. Sci. Technol.* **2012**, *25*, 124004. [CrossRef]
73. Poccia, N.; Fratini, M.; Ricci, A.; Campi, G.; Barba, L.; Vittorini-Orgeas, A.; Bianconi, G.; Aeppli, G.; Bianconi, A. Evolution and control of oxygen order in a cuprate superconductor. *Nat. Mater.* **2011**, *10*, 733–736. [CrossRef]
74. Sidorenko, A.S. Fractal geometry in superconductivity. *Mold. J. Phys. Sci.* **2002**, *1*, 102–105.
75. Gabovich, A.M.; Moiseev, D.P.; Panaitov, G.I.; Sidorenko, A.S.; Postinov, V.M. Relaxation of the magnetization in superconducting oxides. *Mod. Phys. Lett. B.* **1989**, *3*, 1503–1509. [CrossRef]